Anodic activity of boron-doped diamond electrodes in bleaching processes: effects of ultrasound and surface states

Katherine B. Holt,[a] Claire Forryan,[a] Richard G. Compton,[a] John S. Foord*[a] and Frank Marken[b]

[a] *Physical and Theoretical Chemistry Laboratory, Oxford University, Oxford, UK OX1 3QZ*
[b] *Department of Chemistry, Loughborough University, Loughborough, Leicestershire, UK LE11 3TU*

Received (in London, UK) 24th January 2003, Accepted 4th March 2003
First published as an Advance Article on the web 13th March 2003

In this study three types of polycrystalline highly boron-doped (*ca.* 10^{20} cm^{-3}) diamond electrodes are compared with respect to their activity in anodic bleaching processes. A commercially available boron-doped diamond electrode (from De Beers), a conventional polycrystalline boron-doped diamond electrode grown in a hot filament chemical vapour deposition (HFCVD) process, and an sp^2-carbon impurity state-rich polycrystalline boron-doped diamond electrode (grown in the presence of a high methane concentration) are characterized by voltammetry, Raman spectroscopy, and electron microscopy methods. Next, the efficiency of anodic bleaching processes (assumed to be based on hydroxyl radical generation at the diamond electrode surface) is investigated as a function of surface modification and with/without activation by power ultrasound. As a model process, the bleaching of the spin trapping reagent *N*,*N*-dimethyl-*p*-nitrosoaniline (RNO), is employed. Power ultrasound is shown to drastically improve the rate of bleaching by increasing the rate of mass transport at the electrode|solution interface. However, the state of the diamond electrode surface is also important. Boron-doped diamond electrodes rich in sp^2 carbon impurity states are initially more efficient in the bleaching process. Reactive intermediates, such as hydroxyl radicals, appear to be formed preferentially in the vicinity of impurity states. However, mass transport is the dominating parameter in controlling the efficiency of the bleaching process.

1. Introduction

The electro-oxidation of organic molecules has been studied at many electrode materials, such as platinum,[1] carbon felt,[2] PbO_2, Ti/IrO_2 and Ti/SnO_2[3,4] and more recently at boron-doped diamond (BDD)[5–8] among others. A model for anodic oxidation processes within the region of oxygen evolution has been formulated by Comninellis for metal oxide (MO_x) type electrode materials.[9] Surface mediation of the oxidation process is suggested to occur with adsorbed highly reactive intermediates, such as hydroxyl radicals, as the active species. A similar model has been hypothesised for the oxidation of organics at boron-doped diamond (BDD) electrodes. It has been shown that anodic oxidation of organic molecules at boron-doped diamond electrodes in the potential region of simultaneous oxygen evolution can lead to complete, rather than partial/selective oxidation.[10] The properties of boron-doped diamond as an electrode material are unusual and of potential benefit in waste treatment and in electrosynthesis. However, only little is known about the effect of different 'qualities' or 'types' of boron-doped diamond in applications in electrochemistry.

In this report, different types of BDD electrodes are characterised with respect to their ability to bleach organic materials. The bleaching of the spin trap *N*,*N*-dimethyl-*p*-nitrosoaniline (RNO) is assumed here to proceed predominantly *via* reaction with hydroxyl radicals and is employed as an indicator. It has been reported that considerable concentrations of hydroxyl radicals can be formed at high positive potentials at the diamond electrode surface.[5–8] It has been proposed that hydroxyl radical formation could be associated with sp^2 impurity sites on the surface and that diamond with a high graphitic carbon content produces higher quantities of radicals.[11] Here, experiments are described to indirectly quantify the concentration (or flux) of hydroxyl radicals formed at the diamond electrode surface by monitoring the bleaching process. The effects of current density and activation by power ultrasound are studied. The effect of diamond quality was studied in an attempt to confirm that the production of hydroxyl radicals is associated with surface sites of sp^2 character.

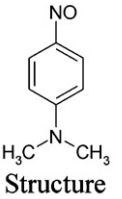

Structure of RNO

2. Experimental

2.1. Reagents

The hydroxyl radical spin trap, *N*,*N*-dimethyl-*p*-nitrosoaniline (RNO) was employed, dissolved in 0.2 M pH 7 phosphate buffer solution (PBS). $Ru(NH_3)_6^{3+}$ was used in aqueous 0.1 M KCl solution to calibrate the effect of power ultrasound on mass transport.[12] All chemicals were purchased from Aldrich in the purest available or analytical grade and used without further purification. Aqueous solutions were prepared in deionised and filtered water with a resistivity of at least 18 MΩ cm. All solutions were de-aerated with argon for at least 10 minutes prior to experiments.

 DOI: 10.1039/b300994g

2.2. Instrumentation

Free-standing 2 mm × 5 mm polycrystalline (type A) BDD electrodes (De Beers, distributed by Windsor Scientific, Slough, UK) were used either as received or modified in a microwave plasma chamber (1200 kW, 5% methane and 95% hydrogen, 10 minutes) to provide a surface layer rich in graphitic impurity states. Boron-doped diamond (BDD) electrodes were also grown in house on tungsten rod substrates (1 mm diameter, 10 mm length) using a hot filament chemical vapour deposition (HFCVD) system, as described previously.[13] High quality (type B) polycrystalline boron-doped diamond electrodes (doping level *ca.* 10^{20} cm^{-3}) were grown using a conventional feed-gas mix of 1% methane to 99% hydrogen. Polycrystalline boron-doped diamond electrodes (type C) rich in graphitic impurity states were grown by increasing the methane content to 3%. Electrical contact with the electrode was achieved by spot-welding a nickel wire to the tungsten substrate and the electrodes were heat-shrink mounted in PTFE holders to prevent leaking.

Electrochemical measurements were carried out with a conventional three-electrode arrangement controlled by a potentiostat (μ-Autolab, Eco Chemie, The Netherlands), with a diamond working electrode (described and characterised below), a platinum coil counter electrode and a saturated calomel reference electrode (SCE). Power ultrasound was introduced using an ultrasound processor (Hielscher UP 200G, 24 kHz, maximum output power approximately 8 W cm^{-2} based on calorimetric calibration) fitted with a 13 mm diameter glass horn. Raman spectra were obtained with a Dilor-Labram spectrometer fitted with an argon laser. Scanning Electron Microscopy (SEM) images were obtained using a JEOL JSM-5200 system.

2.3. Procedures

The different types of BDD electrodes were first characterised using Raman, SEM and cyclic voltammetry and then used in experiments to investigate the bleaching of *N*,*N*-dimethyl-*p*-nitrosoaniline (RNO) at high anodic potentials. RNO is acting as a spin trap (as proposed by Comninellis[14] and Wabner[15]) for the indirect detection of hydroxyl radicals generated at electrodes at high anodic potentials. This spin trap system has been chosen because it appears to react selectively with hydroxyl radicals, and does not react with singlet oxygen or other peroxy compounds.[15] RNO also has been reported to react with a very high essentially diffusion controlled reaction rate with hydroxyl radicals ($k = 1.2 \times 10^{10}$ M^{-1} s^{-1}) and is therefore very sensitive even at low radical concentrations. The detection of the spin adduct can be based on a colour change. The yellow colour of the RNO molecule becomes bleached upon reaction with hydroxyl radicals. The bleaching of the strong adsorption band at 440 nm ($\varepsilon = 3.44 \times 10^4$ M^{-1} cm^{-1}) can therefore be followed quantitatively by using a UV-visible spectrometer.

Electrolysis under 'silent' conditions was carried out in a two-compartment cell, as shown in Fig. 1a, with the working (BDD) electrode and the counter electrode separated by a salt bridge (a U-tube filled with 0.2 M KNO_3 in agar paste). The working electrode compartment contained 3 cm^3 of the aqueous buffer solution containing RNO. Electrolysis experiments in the presence of power ultrasound were carried out in a 40 cm^3 volume cell, with a glass frit separating the counter electrode from the bulk solution (Fig. 1b).

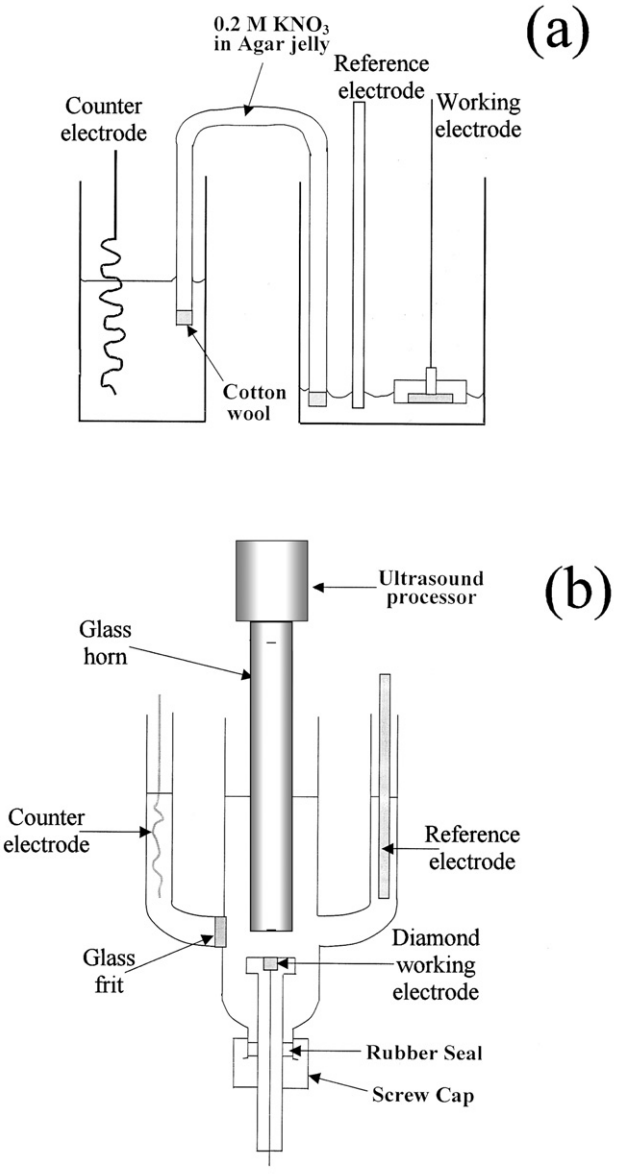

Fig. 1 Schematic of the experimental set-up for electrochemical and RNO bleaching experiments (a) under silent conditions and (b) under ultrasound conditions.

3. Results and discussion

3.1. Voltammetric characterisation of boron-doped diamond electrodes

Three types of boron-doped diamond electrodes were employed in this study: type A polycrystalline boron-doped diamond electrodes obtained from De Beers, type B high quality polycrystalline boron-doped diamond electrodes grown in a HFCVD process, and type C also grown using HFCVD but using a carbon-rich gas mixture.

Fig. 2 shows the first, second, and third consecutive cyclic voltammograms (scan rate 0.1 V s^{-1}) for the oxidation of the surface of a type C boron-doped diamond electrode immersed in 0.2 M PBS at pH 7. The first scan shows characteristic oxidation peaks in the potential region 1.5 V to 2.4 V *vs.* SCE. This surface oxidation is followed at more positive potentials by a current response attributed to the anodic electrolysis of water resulting in the evolution of oxygen. An intermediate in this oxidation reaction is believed to be the hydroxyl radical. The current peaks at 1.5 to 2.4 V *vs.* SCE have been suggested to be associated with the oxidation of graphitic inclusions in the intercrystalline boundaries of the diamond electrode.[16] The height of this peak diminishes in subsequent scans and is almost absent by the third potential scan, as the surface becomes oxidised (see Fig. 2).

Similar cyclic voltammograms were obtained for type A and type B electrodes (not shown), but type C (sp^2-carbon rich)

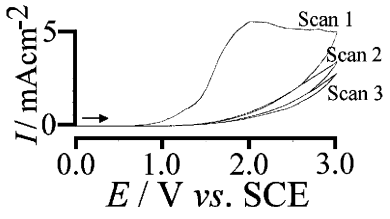

Fig. 2 Three consecutive cyclic voltammograms (scan rate 0.1 V s^{-1}) obtained at a 1 mm diameter type C (sp^2-carbon rich) BDD electrode immersed in aqueous 0.2 M phosphate buffer solution at pH 7.

electrodes showed the most prominent oxidation currents. The large size of this oxidation signal suggests the presence of more surface sp^2 sites available for oxidation processes. The second and third scans show that this current response is much decreased after the first scan, which indicates that some change to the surface has taken place. The oxidation peaks in this potential region can be taken as an approximate measure of the sp^2-carbon impurity states at the electrode surface. The surface composition of the electrodes will be discussed in more detail further below.

3.2. The bleaching process

The effect of applied anodic current density on the amount of RNO bleached was investigated first employing a 2 mm × 5 mm BDD electrode (type A) immersed in 3 cm^3 aqueous 0.2 M PBS containing 2×10^{-5} M RNO. In order to investigate the possibility that bleaching might occur through the direct oxidation of RNO *via* electron transfer at the electrode surface, background voltammograms were recorded in the range of electrolyte stability for the BDD electrode in 0.2 M PBS at pH 7. The voltammograms (not shown) were identical with voltammograms obtained in the absence of RNO, which suggests that direct oxidation of RNO does not take place at BDD electrodes within the potential region of electrolyte stability.

Fig. 3 shows the percentage of RNO bleached after 30 min at current densities of 1, 5, 10 and 20 mA cm^{-2} for the BDD electrode. The amount of RNO bleached shows an approximately linear increase with increasing current density beyond a threshold of 5 mA cm^{-2}. At lower current densities the bleaching efficiency remains approximately constant (see dashed line). The bleaching of RNO is assumed to be associated with hydroxyl radical generation at the working electrode. A suggested mechanism for the decomposition of the solvent at anodic potentials is a one-electron oxidation of water molecules at active surface sites on the electrode resulting in the formation of adsorbed hydroxyl radical

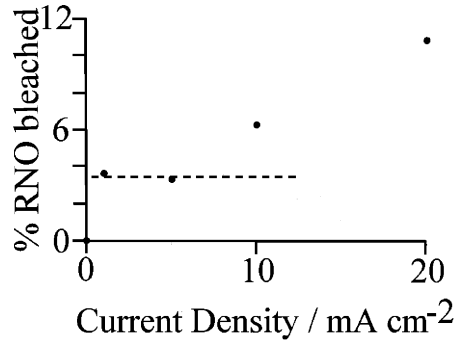

Fig. 3 Plot of the percentage of RNO bleached (in 3 cm^3 solution containing initially 2×10^{-5} M RNO in aqueous 0.2 M phosphate buffer at pH 7) after 30 min bleaching at different anodic current densities at a 2 mm × 5 mm BDD (type A) electrode.

Table 1 Data for the bleaching of 2×10^{-5} M RNO (in 3 cm^3 aqueous 0.2 M PBS at pH 7, 30 min) at a 2 mm × 5 mm BDD (type A) electrode. An efficiency of 100% corresponds to one molecule bleached per electron transferred

Current density/ mA cm^{-2}	RNO bleached (%)	Experimental efficiency (%)	Theoretical efficiency (%)
1	3.8	0.122	0.1
5	3.6	0.024	0.02
10	6.2	0.019	0.01
20	10.4	0.017	0.005

intermediates.[9,10] Based on this mechanism, initially an increase of the bleaching efficiency with current density is expected followed by 'saturation' at a threshold value consistent with the mass transport limited rate. The dashed line in Fig. 3 indicates the mass transport limited rate (*vide infra*). The increase at high current densities may be attributed to a mass transport effect introduced by gas bubbles during oxygen evolution at higher current densities.

Table 1 shows calculated values for the efficiency of the bleaching process. The efficiency of the process is defined here as the number of molecules of RNO bleached (in %) for every electron passed. It can be seen that the efficiency is relatively low with less than one in every thousand electrons passed resulting in bleaching. The process is dominated by oxygen evolution.

It is interesting to compare the observed experimental efficiency with that expected for a mass transport controlled process. Eqn. 1 allows the 'theoretical efficiency' to be estimated based on the assumption of a one electron process, Faraday's constant F, the bulk RNO concentration c, the estimated[17] diffusion coefficient for RNO in water of approximately $D = 0.67 \times 10^{-9}$ m^2 s^{-1}, and a Nernst diffusion layer thickness of approximately $\delta = 150$ μm (in the presence of natural convection only).

$$\text{Efficiency (in \%)} = \frac{I_{\text{mass transport limited}}}{I_{\text{experimental}}} \times 100 = \frac{F D c}{\delta I_{\text{experimental}}} \times 100 \quad (1)$$

For a current density of $I_{\text{experimental}} = 1$ mA cm^{-2} the theoretical efficiency can be calculated as approximately 0.1% in agreement with the result given in Table 1. The higher experimental efficiency at increased current densities can be attributed to effects of gas evolution on the average diffusion layer thickness.

3.3. The effect of power ultrasound on the bleaching process

The above results suggest that the efficiency of the RNO bleaching process is limited by the mass transport of the RNO to the electrode surface, which means that only a small fraction of the $OH^{\bullet}$ formed at the electrode|solution interface goes on to react with RNO. The application of power ultrasound during electrochemical processes is known to dramatically increase the mass transport of reactants to the electrode surface, through the mechanisms of acoustic streaming and cavitation.[18,19] The average rate of mass transport in the presence of power ultrasound can be conveniently expressed in terms of the diffusion layer thickness, δ. The diffusion layer thickness can be determined, at least approximately, from the value of the limiting current observed for the reduction of $Ru(NH_3)_6^{3+}$ under ultrasound conditions.[19] With the electrodes employed here, a 7 mm electrode-to-horn separation, and with 4 W cm^{-2} ultrasound intensity, the diffusion layer thickness is typically $\delta = 1$ μm.[12]

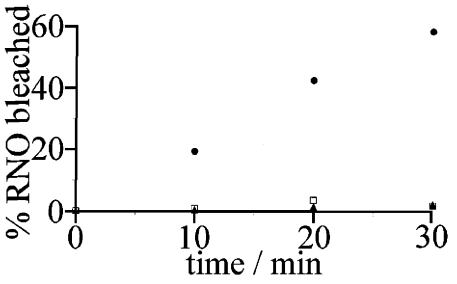

Fig. 4 Plot of percentage of RNO bleached (in 20 cm^3 solution containing initially 2×10^{-5} M RNO in aqueous 0.2 M phosphate buffer at pH 7) at a 2 mm × 5 mm BDD (type A) electrode *versus* time. Black circles: 10 mA cm^{-2} applied current density, 4 W cm^{-2} ultrasound, 7 mm horn–electrode separation; open squares: 4 W cm^{-2} ultrasound only, 7 mm horn–electrode separation; black triangles: 10 mA cm^{-2} applied current density only.

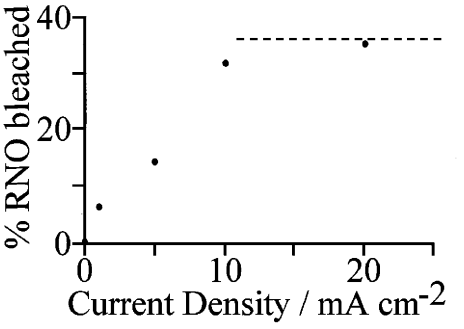

Fig. 5 Plot of percentage of RNO bleached (in 20 cm^3 solution containing initially 2×10^{-5} M RNO in aqueous 0.2 M phosphate buffer at pH 7) at a 2 mm × 5 mm BDD (type A) electrode after 15 min with 4 W cm^{-2} applied ultrasound (horn–electrode separation 7 mm) as a function of current density.

It has been reported that the use of ultrasound in aqueous solutions can facilitate the formation of hydroxyl radicals by the sonolytic cleavage of water molecules during the collapse of cavitation bubbles.[20] In order to investigate this possibility, a control experiment was carried out, in which 4 W cm^{-2} ultrasound was applied to 20 cm^3 of a solution of RNO in aqueous buffer under zero current conditions. Also an additional experiment was carried out, which involved the application of a current density of 10 mA cm^{-2} to the same volume of solution, but in the absence of ultrasound. Finally, the effect of combining the application of ultrasound to the electrode with a constant anodic current density of 10 mA cm^{-2} was investigated. The results shown in Fig. 4 demonstrate the dramatic effect ultrasound has on the bleaching process.

A small quantity (3%) of RNO is bleached with the application of 10 mA cm^{-2} anodic current density under silent conditions (black triangles) after 30 min. The application of ultrasound in the absence of current results in the bleaching of a comparably small amount of RNO (~3% after 30 min). This appears to confirm that a small quantity of $OH^{\bullet}$ is produced by the sonolytic cleavage of water bonds in the presence of power ultrasound. A dramatic increase in the amount of RNO bleaching is observed for the combination of 10 mA cm^{-2} anodic current density with 4 W cm^{-2} ultrasound. There is a twenty-fold increase in the amount of RNO bleached after 30 minutes under sonication in comparison to the silent experiment. The reason for this is likely to be increased mass transport of RNO molecules to the electrode surface, resulting in an increased rate of encounter between the dissolved RNO species and the hydroxyl radicals.

Further effects may play a role, such as the prevention of bubble formation (which accompanies the gas evolution reaction) by the turbulent hydrodynamic forces induced by ultrasound. Ultrasound may also 'activate' the electrode surface in other ways, for example in preventing the adsorption of RNO molecules, or efficiently removing the hydroxylated products from the electrode surface.

Further experiments were carried out with the application of power ultrasound, using different current densities. Bleaching experiments employing 20 cm^3 of 2×10^{-5} M RNO were carried out, with current densities of 1, 5, 10 and 20 mA cm^{-2}, for 15 min each. The results are shown in Fig. 5. The general trend is that of a non-linear increase in the percentage of bleaching with current density. The quantity of RNO bleached increases almost linearly for current densities of 1, 5 and 10 mA cm^{-2}. At a higher current density of 20 mA cm^{-2} the amount of bleaching is limiting off, which could suggest that the reaction becomes mass transport limited at sufficiently high current densities (see dashed line).

The values of percentage RNO bleached and efficiency of the bleaching process were calculated as described previously, and are presented in Table 2. Comparison with Table 1 for values of efficiency obtained for identical experiments in the absence of ultrasound illustrates the dramatic increase in efficiency achieved when ultrasound is applied to the electrode during bleaching. At 20 mA cm^{-2} the percentage of RNO bleaching has not increased much from the value at 10 mA cm^{-2}, as the process has become mass transport limited. From this limit in mass transport of RNO to the electrode surface can be obtained (i) first the flux of RNO towards the electrode surface, corresponding to *ca.* 0.13 mA cm^{-2} (see onset of mass transport limited conditions in Fig. 5), and (ii) next the average diffusion layer thickness in the presence of ultrasound, approximately $\delta = 1$ μm, in good agreement with the estimate based on electrochemical experiments (*vide supra*).

With the diffusion layer thickness estimated, the theoretical efficiencies (see eqn. 1) can be calculated for the ultrasound activated processes and are included in Table 2. Deviations of the 'experimental efficiencies' from the 'theoretical efficiencies' are due to kinetic effects *e.g.* the limited availability of hydroxyl radicals for reaction with RNO due to competition with oxygen evolution.

3.4. The effect of diamond electrode growth conditions and surface composition on bleaching

The cyclic voltammograms shown in Fig. 2 suggest that the growth conditions for the diamond electrodes change the surface properties and this may result in different behaviour during oxidation or bleaching processes. To explore this type of effect, two different types of electrodes were grown under controlled conditions in a CVD reactor. The first type of electrode, type B, was standard good quality polycrystalline BDD grown on a 1 mm diameter tungsten substrate, with a feed gas mixture of 1% CH_4:99% H_2. This electrode consists of crystallites of the order of 10 μm, as shown in the SEM image in Fig. 6a, and has very little graphitic sp^2 content, as shown by the Raman spectrum in Fig. 7a. The second type of electrode, type C, was grown with a carbon-rich gas mixture of 3% CH_4:97%

Table 2 Data for the bleaching of 2×10^{-5} M RNO (in 20 cm^3 aqueous 0.2 M PBS at pH 7, 15 min) at a 2 mm × 5 mm BDD (type A) electrode in the presence of 4 W cm^{-2} ultrasound

Current density/ mA cm^{-2}	RNO bleached (%)	Experimental efficiency (%)	Theoretical efficiency (%)
1	6.5	2.78	17
5	14.0	1.19	3.4
10	32.0	1.36	1.7
20	34.0	0.73	0.8

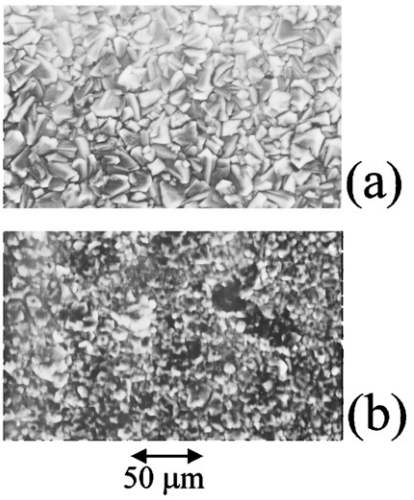

Fig. 6 SEM images of (a) high quality polycrystalline boron-doped diamond (type B) and (b) sp^2-carbon-rich polycrystalline boron-doped diamond (type C).

H_2, resulting in an sp^2-carbon rich diamond, as illustrated by the occurrence of a pronounced graphite peak at ~1550 cm^{-1} in the Raman spectrum (Fig. 7b). The crystallites for the sp^2-carbon rich boron-doped diamond are also smaller, of the order 5 μm (see Fig. 6b) indicating the presence of more grain boundaries.

RNO bleaching experiments were carried out using each electrode in 3 cm^3 aqueous 0.2 M PBS at pH 7 containing 2×10^{-5} M RNO. A current density of 30 mA cm^{-2} was employed to increase the sensitivity of the bleaching process. The amount of bleaching with time was monitored and data are plotted in Fig. 8. The results show that the amount of RNO bleached for both electrodes increases linearly with time. However, the initial bleaching rate is higher at the sp^2-carbon rich (type C) electrode, where 7.8% of the RNO has been bleached after 5400 s compared to 6.8% at the high quality type B electrode. This suggests that there is a correlation between the initial bleaching rate and the surface composition. However, during the bleaching process both types of surfaces become similar in efficiency.

The influence of surface composition of diamond on the bleaching process (or on the quantity of hydroxyl radicals produced at high anodic potentials) was investigated further

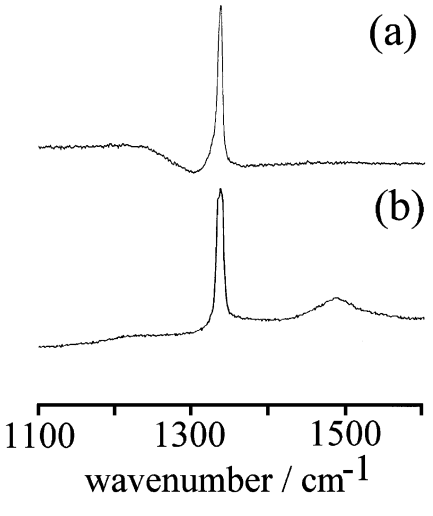

Fig. 7 Raman spectra of (a) high quality polycrystalline boron-doped diamond (type B) and (b) sp^2-carbon-rich polycrystalline boron-doped diamond (type C).

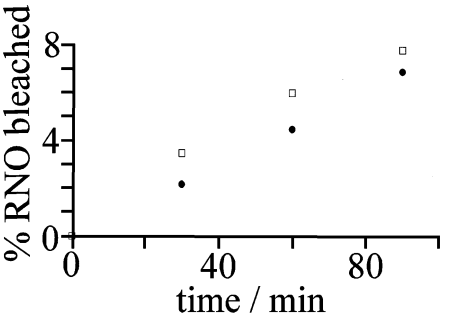

Fig. 8 Plot of the percentage of RNO bleached (in 3 cm^3 solution containing initially 2×10^{-5} M RNO in aqueous 0.2 M phosphate buffer at pH 7, with 30 mA cm^{-2} anodic current density) *versus* time. Black circles: type B electrode, 1 mm diameter high quality BDD on W substrate; open squares: type C electrode, 1 mm diameter carbon-rich BDD electrode on W substrate.

by using a surface modification technique. Microwave plasma treatment was used to bring about changes to the surface chemistry of the De Beers (type A) electrode. A methane/hydrogen microwave plasma is often used for the deposition of diamond. However, in this case, a carbon-rich gas mixture was used for the deposition of an sp^2-carbon rich layer onto the high quality BDD substrate. The diamond sample was first treated with a hydrogen plasma, to clean the surface and provide hydrogen termination. Methane gas was then introduced into the plasma chamber and the diamond surface was treated for 10 minutes with a 5% CH_4:95% H_2 feed gas mixture at 35 Torr and 600 °C with a microwave power of 1200 kW. The surface was only treated for a short period of time to cause deposition of a very thin layer of graphitic carbon. The sample was then cooled under a flow of hydrogen before the BDD electrode was used for three consecutive RNO bleaching experiments. The results for these experiments conducted in 3 cm^3 aqueous 0.2 M PBS containing RNO for 30 min each time are summarised in Table 3. The results show a dramatic increase in the amount of RNO bleaching (35.5%) after the treatment of the diamond surface with a carbon-rich plasma. This can be compared to the value of 7.3% on average obtained for an untreated type A electrode under the same conditions. This clearly illustrates that the introduction of sp^2-carbon to the surface of the electrode results in an increase in the efficiency of bleaching of RNO. This suggests that the sp^2 impurity sites may be directly associated with the formation of hydroxyl radicals. The 2nd and 3rd experiments show a decrease in the amount of RNO bleached, which is indicative of oxidation of the surface and passivation of the active sites.

4. Conclusion

A radical spin trapping reagent, RNO, has been employed to monitor bleaching and the formation of reactive intermediates

Table 3 Data for the bleaching of 2×10^{-5} M RNO (in 3 cm^3 0.2 M PBS at pH 7) in 30 min with 10 mA cm^{-2} current density for three consecutive experiments after surface modification of the 2 mm × 5 mm BDD (type A) electrode with 5% CH_4:95% H_2 microwave powered plasma (600 °C, 35 Torr, 1200 kW)

	RNO bleached (%)
1st Bleaching experiment after CH_4/H_2 plasma treatment	35.5
2nd Bleaching experiment after CH_4/H_2 plasma treatment	13.1
3rd Bleaching experiment after CH_4/H_2 plasma treatment	6.9

such as hydroxyl radicals at different types of boron-doped diamond electrodes. Both the surface state of the diamond electrodes and the mass transport at the electrode|solution interface have dramatic effects on the rate of bleaching. Introducing sp^2-carbon impurities at the diamond surface enhanced the bleaching rate only in the initial stages of the oxidation process probably due to oxidation of states themselves. Introducing fast mass transport by applying power ultrasound during the bleaching process allows the bleaching rate to be increased up to the mass transport controlled limit. However, in order to achieve mass transport control, a very high current density has to be applied, which reduces the efficiency of the overall process to about 1% (in the presence of 2×10^{-5} M RNO).

Acknowledgements

F.M. thanks the Royal Society for a University Research Fellowship. The EPSRC (GR/N 12015) is gratefully acknowledged for financial support.

References

1 D. C. Johnson, J. Feng and L. L. Houk, *Electrochim. Acta*, 2000, **46**, 323.
2 A. M. Polcaro and S. Palmas, *Ind. Eng. Chem. Res.*, 1997, **36**, 1791.
3 J. D. Rodgers, W. Jedral and N. I. Bunce, *Environ. Sci. Technol.*, 1999, **33**, 1453.
4 C. Pulgarin, N. Adler, P. Peringer and C. Comninellis, *Water Res.*, 1994, **28**, 887.
5 J. Iniesta, P. A. Michaud, M. Panizza, G. Cerisola, A. Aldaz and C. Comninellis, *Electrochim. Acta*, 2001, **46**, 3573.
6 M. A. Rodrigo, P. A. Michaud, I. Duo, M. Panizza, G. Cerisola and C. Comninellis, *J. Electrochem. Soc.*, 2001, **148**, D60.
7 P. L. Hagans, P. M. Natishan, B. R. Stoner and W. E. O'Grady, *J. Electrochem. Soc.*, 2001, **148**, E298.
8 A. J. Saterlay, J. S. Foord and R. G. Compton, *Electroanalysis*, 2001, **13**, 1065.
9 O. Simond, V. Schaller and C. Comninellis, *Electrochim. Acta*, 1997, **42**, 2009.
10 G. Foti, D. Gandini, C. Comninellis, A. Perret and W. Haenni, *Electrochem. Solid State Lett.*, 1999, **2**, 228.
11 M. D. Koppang, M. Witek, J. Blau and G. M. Swain, *Anal. Chem.*, 1999, **71**, 1188.
12 See for example K. B. Holt, J. Del Campo, J. S. Foord, R. G. Compton and F. Marken, *J. Electroanal. Chem.*, 2001, **513**, 94.
13 C. H. Goeting, F. Marken, A. Guitierrez-Sosa, R. G. Compton and J. S. Foord, *New Diam. Front. Carbon Technol.*, 1999, **9**, 207.
14 C. Comninellis, *Electrochim. Acta*, 1994, **39**, 1857.
15 D. Wabner and C. Grambow, *J. Electroanal. Chem.*, 1985, **195**, 95.
16 H. B. Martin, A. Argoitia, U. Landau, A. B. Anderson and J. C. Angus, *J. Electrochem. Soc.*, 1996, **143**, L133.
17 C. R. Wilke and P. Chang, *AIChE J.*, 1955, **1**, 264.
18 D. J. Walton and S. S. Phull, *Adv. Sonochem.*, 1996, **4**, 205.
19 R. G. Compton, J. C. Eklund and F. Marken, *Electroanalysis*, 1997, **9**, 509.
20 See for example M. R. Hoffmann, I. Hua and R. Hochemer, *Ultrason. Sonochem.*, 1996, **3**, S163.